

## The Origin of Chemo- and Enantioselectivity in the Hydrogenation of Diketones on Platinum

Simon Diezi, Davide Ferri, Angelo Vargas, Tamas Mallat, and Alfons Baiker\*

Contribution from the Department of Chemistry and Applied Biosciences, ETH Zurich, Hönggerberg, HCI, CH-8093 Zurich, Switzerland

Received November 7, 2005; E-mail: baiker@chem.ethz.ch

**Abstract:** In the Pt-catalyzed hydrogenation of 1,1,1-trifluoro-2,4-diketones, addition of trace amounts of cinchonidine, *O*-methyl-cinchonidine, or (*R,R*)-pantoyl-naphthylethylamine induces up to 93% ee and enhances the chemoselectivity up to 100% in the hydrogenation of the activated carbonyl group to an OH function. A combined catalytic, NMR and FTIR spectroscopic, and theoretical study revealed that the two phenomena are coupled, offering the unique possibility for understanding the substrate–modifier–metal interactions. The high chemo- and enantioselectivities are attributed to the formation of an ion pair involving the protonated amine function of the chiral modifier and the enolate form of the substrate. DFT calculations including the simulation of the interaction of a protonated amine with the enolate adsorbed on a Pt 31 cluster revealed that only the C–O bond next to the CF<sub>3</sub> group of the substrate is in direct contact with Pt and can be hydrogenated. The present study illustrates the fundamental role played by the metal surface and indicates that also the enol form can be the reactive species in the hydrogenation of the activated ketone on chirally modified Pt.

### Introduction

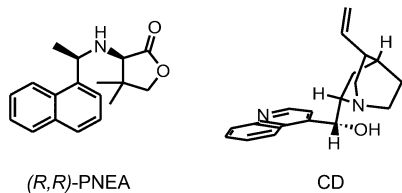
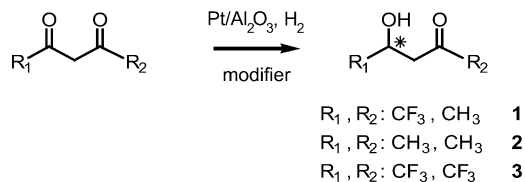
Various strategies have been developed for the creation of chiral surface structures that combine high catalytic activity and stereochemical control.<sup>1–5</sup> Among them, imparting chirality to a catalytic active metal surface by adsorption of chiral organic molecules (chiral modifiers) seems to be one of the most promising.<sup>6–8</sup> This heterogeneous catalytic approach even allows continuous process operation.<sup>9–11</sup> In the hydrogenation of C=O and C=C functions, chirally modified supported metal catalysts represent a successful approach with synthetic potential.<sup>12–20</sup>

An emerging field is the Pt-catalyzed enantioselective hydrogenation of  $\alpha,\alpha,\alpha$ -trifluoromethyl ketones to chiral fluori-

nated alcohols,<sup>21–24</sup> the compounds of which have attracted great attention in past years in agro- and pharmaceutical chemistry.<sup>25,26</sup> Although the ee's are frequently lower than those achieved in homogeneous catalysis,<sup>27,28</sup> the supported metal catalyst (usually Pt/Al<sub>2</sub>O<sub>3</sub>) and the cinchona alkaloids used as modifiers are cheap and commercially available, and the technical handling is not demanding. Thoroughly investigated substrate groups are aromatic trifluoromethyl ketones<sup>29,30</sup> and aliphatic ketones possessing an additional (nonactivated) carbonyl group in the  $\beta$ -position.<sup>31–33</sup> At best, 92% ee was achieved in the hydrogenation of 2,2,2-trifluoroacetophenone<sup>30</sup> and 96% ee in the hydrogenation of ethyl-4,4,4-trifluoroacetoacetate.<sup>34</sup> The best chiral modifiers for Pt are the naturally occurring cinchonidine (CD), its *O*-methyl-derivative (MeOCD), and the synthetic modifier (*R,R*)-pantoyl-naphthylethylamine ((*R,R*)-PNEA). Recently, the latter modifier afforded better than 99% chemoselectivity and

- (1) Baiker, A. *Curr. Opin. Solid State Mater. Sci.* **1998**, *3*, 86.
- (2) Bein, T. *Curr. Opin. Solid State Mater. Sci.* **1999**, *4*, 85.
- (3) Sherrington, D. C. *Catal. Today* **2000**, *57*, 87.
- (4) Davis, M. E. *Top. Catal.* **2003**, *25*, 3.
- (5) McMorn, P.; Hutchings, G. J. *Chem. Soc. Rev.* **2004**, *33*, 108.
- (6) Bürgi, T.; Baiker, A. *Acc. Chem. Res.* **2004**, *37*, 909.
- (7) Murzin, D. Y.; Mäki-Arvela, P.; Toukonniitty, E.; Salmi, T. *Catal. Rev.-Sci. Eng.* **2005**, *47*, 175.
- (8) Baiker, A. *Catal. Today* **2005**, *100*, 159.
- (9) Künzle, N.; Hess, R.; Mallat, T.; Baiker, A. *J. Catal.* **1999**, *186*, 239.
- (10) Baiker, A.; Künzle, N.; Mallat, T. EP1063224, Hoffmann La Roche, December 27, 2000.
- (11) Toukonniitty, E.; Mäki-Arvela, P.; Kalantar Neyestanaki, A.; Salmi, T.; Murzin, D. Y. *Appl. Catal., A* **2002**, *235*, 125.
- (12) Wells, P. B.; Wilkinson, A. G. *Top. Catal.* **1998**, *5*, 39.
- (13) Sugimura, T. *Catal. Surv. Jpn.* **1999**, *3*, 37.
- (14) Baiker, A. *J. Mol. Catal. A: Chem.* **2000**, *163*, 205.
- (15) Osawa, T.; Harada, T.; Takayashu, O. *Top. Catal.* **2000**, *13*, 155.
- (16) Török, B.; Balázsik, K.; Felföldi, K.; Bartók, M. *Ultrason. Sonochem.* **2001**, *8*, 191.
- (17) von Arx, M.; Mallat, T.; Baiker, A. *Top. Catal.* **2002**, *19*, 75.
- (18) Baddeley, C. J. *Top. Catal.* **2003**, *25*, 17.
- (19) Studer, M.; Blaser, H.-U.; Exner, C. *Adv. Synth. Catal.* **2003**, *345*, 45.
- (20) Sipos, E.; Tungler, A.; Fogassy, G. *J. Mol. Catal. A: Chem.* **2004**, *216*, 171.
- (21) Balázsik, K.; Török, B.; Felföldi, K.; Bartók, M. *Ultrason. Sonochem.* **1999**, *5*, 149.
- (22) von Arx, M.; Mallat, T.; Baiker, A. *Angew. Chem., Int. Ed.* **2001**, *40*, 2302.
- (23) Varga, T.; Felföldi, K.; Forgó, P.; Bartók, M. *J. Mol. Catal. A: Chem.* **2004**, *216*, 181.
- (24) Felföldi, K.; Varga, T.; Forgó, P.; Bartók, M. *Catal. Lett.* **2004**, *97*, 65.
- (25) Hudlicky, M. *Chemistry of Organic Fluorine Compounds*; Ellis Horwood Ltd.: Chichester, 1992.
- (26) Filler, R.; Kobayashi, Y.; Yagupolskii, L. M. *Organofluorine Compounds in Medicinal Chemistry and Biomedical Applications*; Elsevier: Amsterdam, 1993.
- (27) Kuroki, Y.; Asada, D.; Iseki, K. *Tetrahedron Lett.* **2000**, *41*, 9853.
- (28) Kuroki, Y.; Sakamaki, Y.; Iseki, K. *Org. Lett.* **2001**, *3*, 457.
- (29) Mallat, T.; Bodmer, M.; Baiker, A. *Catal. Lett.* **1997**, *44*, 95.
- (30) von Arx, M.; Mallat, T.; Baiker, A. *Tetrahedron: Asymmetry* **2001**, *12*, 3089.
- (31) von Arx, M.; Mallat, T.; Baiker, A. *J. Catal.* **2000**, *193*, 161.
- (32) Hess, R.; Diezi, S.; Mallat, T.; Baiker, A. *Tetrahedron: Asymmetry* **2004**, *15*, 251.
- (33) Diezi, S.; Hess, M.; Orglmeister, E.; Mallat, T.; Baiker, A. *J. Mol. Catal. A: Chem.* **2005**, *239*, 49.
- (34) von Arx, M.; Mallat, T.; Baiker, A. *Catal. Lett.* **2002**, *78*, 267.

**Scheme 1.** Hydrogenation of (Fluorinated)  $\beta$ -Diketones over Pt/Al<sub>2</sub>O<sub>3</sub> Modified by Me<sub>3</sub>N, Et<sub>3</sub>N, Quinuclidine, Quinoline, (R,R)-PNEA, CD, and O-Methyl-CD



93% ee in the hydrogenation of 1,1,1-trifluoro-acetylacetone (**1**, Scheme 1) to the corresponding alcohol.<sup>35</sup>

Despite the impressive development in this field in the past years, the mechanistic details at the base of the reaction are still under debate. Several models have been developed, and the conflicting opinions reflect the great scientific interest of this topic.<sup>23,24,36,37</sup> There is some agreement on the formation of chiral sites on the metal surface upon adsorption of the modifier, and also on 1:1 interactions between adsorbed modifier and substrate.<sup>38</sup> However, contrasting hypotheses have been formulated concerning the nature of substrate–modifier interactions that lead to selectivity during hydrogenation of activated ketones on Pt. Because the basic N atom of the modifier is in most cases crucial for enantiodifferentiation (with only one known exception<sup>39</sup>), interaction models have clustered around the two main roles that can be played by this function: (i) hydrogen-bond donor to the keto-carbonyl oxygen after protonation,<sup>38,40</sup> and (ii) nucleophile to the keto-carbonyl carbon as free amine.<sup>23,37,41</sup> Steric effects are generally considered crucial for selectivity, after formation of one of the aforementioned interactions. It has also been proposed that the ketone might interact via hydrogen bonding with the adsorbed aromatic anchoring group.<sup>42</sup> In this proposal, the anchoring group would then become a second docking site, but the relevance of such interactions still has to be proven. On the other hand, catalytic and basic organic chemistry studies questioned recently the role of quinuclidine as a nucleophile,<sup>43,44</sup> whereas the 1:1 model operating via hydrogen bond seems to become an increasingly durable concept. With this background, any experimental observation that can shed some light on the nature of the 1:1 interactions between the ketone substrate and the chiral amine modifier is of great interest for rationalization of the catalyst

action. A major limitation of heterogeneous enantioselective catalysis is that truly in situ spectroscopic studies<sup>45,46</sup> supporting the mechanistic models are barely available due to technical difficulties.

Hydrogenation of fluorinated  $\beta$ -diketones revealed that addition of the chiral amine or amino alcohol-type modifier not only induced enantioselection but also enhanced the low chemoselectivity to 99–100% in the hydrogenation of the activated keto function.<sup>32,33,35</sup> Similar observations have been reported for the hydrogenation of  $\alpha,\gamma$ -diketoesters,<sup>47</sup> and no explanation for the excellent chemoselectivity has been found yet. We assumed that chemo- and enantioselectivities in the hydrogenation of fluorinated  $\beta$ -diketones are coupled phenomena, and understanding how the modifier enhances the chemoselectivity can lead us to the mechanism of enantioselection. The following mechanistic study based on catalytic experiments, NMR and FTIR spectroscopic data, and high-level calculations, indicates that the acid–base-type substrate–modifier interaction is strongly affected by the adsorption on the metal surface.

## Experimental Section

**Materials.** 1,1,1-Trifluoro-2,4-pentanedione **1** (Acros), acetylacetone **2** (Fluka) and 3-penten-2-one **4** (Alfa Aesar) were distilled before use. Toluene (J. T. Baker) was dried and stored over activated molecular sieves. Trimethylamine (Me<sub>3</sub>N, Fluka), triethylamine (Et<sub>3</sub>N, Fluka), quinoline (Fluka), quinuclidine (Aldrich), trifluoroacetic acid (TFA, Fluka), cinchonidine (CD, Fluka), and 1,1,1,5,5,5-hexafluoroacetylacetone **3** (Acros) were used as received. O-Methyl-cinchonidine (MeOCD)<sup>48</sup> and (R,R)-pantoyl-naphthylethylamine ((R,R)-PNEA, Scheme 1)<sup>49</sup> were synthesized by known procedures. The 5 wt % Pt/Al<sub>2</sub>O<sub>3</sub> (E4759) catalyst was purchased from Engelhard.

**Catalytic Hydrogenations.** The hydrogenation reactions were carried out in a mechanically stirred parallel pressure reactor system (Argonaut Technologies) or in a magnetically stirred stainless steel autoclave controlled by computerized constant-volume constant-pressure equipment (Büchi BPC 9901). Optimally, the 5 wt % Pt/Al<sub>2</sub>O<sub>3</sub> catalyst was prereduced before use in a fixed-bed reactor by flushing with N<sub>2</sub> at 400 °C for 30 min, followed by reductive treatment in H<sub>2</sub> for 60 min at the same temperature. After being cooled to room temperature in H<sub>2</sub> (30 min), the catalyst was directly used for hydrogenation. The metal dispersion was 0.32 and 0.20 before and after reductive heat treatment, respectively, as calculated from the average particle size determined by TEM.<sup>50</sup> According to standard conditions, 42 mg of catalyst, 1.84 mmol of substrate, 6.8  $\mu$ mol of modifier, and 5 mL of solvent were stirred (1000 rpm) at 10 bar and room temperature (23–25 °C) for 2 h. Deviations from the standard conditions are specified in the text.

Conversion and enantiomeric excess (ee) were determined by gas chromatography using a Chirasil-DEX CB column (Chrompack). The products were identified via GC/MS (HP 5973 mass spectrometer) and NMR. The enantiomers were verified by comparing the sign of their optical rotation (Perkin-Elmer 241 polarimeter) with literature data.<sup>51,52</sup> In the hydrogenation of **1**, (R,R)-PNEA, CD, and MeOCD always afforded the (S)-enantiomer in excess, and in the hydrogenation of **2** the (R)-enantiomer formed in slight excess.

(35) Diezi, S.; Hess, M.; Orglmeister, E.; Mallat, T.; Baiker, A. *Catal. Lett.* **2005**, *102*, 121.

(36) Baiker, A. *J. Mol. Catal. A: Chem.* **1997**, *115*, 473.

(37) Vayner, G.; Houk, K. N.; Sun, Y. K. *J. Am. Chem. Soc.* **2004**, *126*, 199.

(38) Schwalm, O.; Minder, B.; Weber, J.; Baiker, A. *Catal. Lett.* **1994**, *23*, 271.

(39) Orglmeister, E.; Mallat, T.; Baiker, A. *J. Catal.* **2005**, *233*, 333.

(40) Blaser, H. U.; Jalett, H. P.; Monti, D. M.; Baiker, A.; Wehrli, J. T. *Stud. Surf. Sci. Catal.* **1991**, *67*, 147.

(41) Augustine, R. L.; Tanielyan, S. K.; Doyle, L. K. *Tetrahedron: Asymmetry* **1993**, *4*, 1803.

(42) Lavoie, S.; Laliberté, M. A.; McBreen, P. H. *J. Am. Chem. Soc.* **2003**, *125*, 15756.

(43) Orglmeister, E.; Mallat, T.; Baiker, A. *J. Catal.* **2005**, *234*, 242.

(44) Vargas, A.; Ferri, D.; Baiker, A. *J. Catal.* **2005**, *236*, 1.

(45) Bonalumi, N.; Bürgi, T.; Baiker, A. *J. Am. Chem. Soc.* **2003**, *125*, 13342.

(46) Schneider, M. S.; Urakawa, A.; Grunwaldt, J.-D.; Bürgi, T.; Baiker, A. *Chem. Commun.* **2004**, 744.

(47) Studer, M.; Burkhardt, S.; Indolese, A. F.; Blaser, H. H. *Chem. Commun.* **2000**, 1327.

(48) Borszky, K.; Bürgi, T.; Zhaoui, Z.; Mallat, T.; Baiker, A. *J. Catal.* **1999**, *187*, 160.

(49) Orglmeister, E.; Mallat, T.; Baiker, A. *Adv. Synth. Catal.* **2005**, *347*, 78.

(50) Hess, R.; Krumeich, F.; Mallat, T.; Baiker, A. *Catal. Lett.* **2004**, *92*, 141.

(51) Forni, A.; Moretti, I.; Prati, F.; Torre, G. *Tetrahedron* **1994**, *50*, 11995.

(52) Besse, P.; Ciblat, S.; Canet, J. L.; Troin, Y.; Veschambre, H. *Tetrahedron: Asymmetry* **2000**, *11*, 2045.

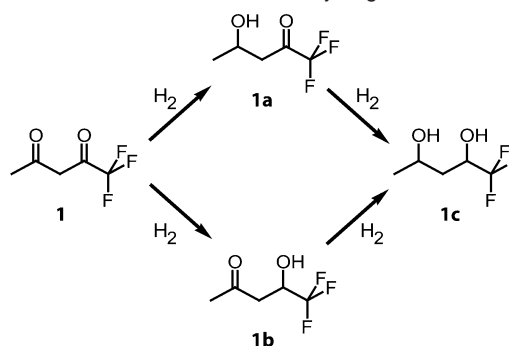
**Spectroscopy.** Protonation of quinuclidine by TFA and the influence of quinuclidine on the keto–enol ratio of **1** have been investigated by  $^1\text{H}$  and  $^{13}\text{C}$  NMR. All NMR data were recorded on a Bruker Avance 500 with TMS as internal standard. The concentration of **1** mimics the conditions in the general reaction procedure (0.37 mol/L).

Transmission infrared spectra were acquired with an IFS66 spectrometer (Bruker Optics) equipped with a DTGS detector. Spectra of quinuclidine/**1** solutions in  $\text{CH}_2\text{Cl}_2$  with increasing molar ratios were recorded using a KBr cell with 1 mm path length. Similar experiments were carried out with **2** and **3**. For comparison, CD was also used.

**Computational Methods.** All calculations of theoretical infrared spectra were performed with the Gaussian 98 set of programs,<sup>53</sup> using density functional theory (DFT) with a hybrid functional (B3LYP) and a 6-31Gdp basis set.

Adsorption studies have been performed using the Amsterdam Density Functional (ADF) program package,<sup>54</sup> and the surface was simulated using a Pt 31 cluster for which the spin state was optimized ( $\alpha - \beta = 8$ ). A frozen core approximation was used for the description of the inner core of the atoms. The orbitals up to 1s were kept frozen for the second row elements, while orbitals up to 4f were kept frozen for platinum. Decreasing the Pt frozen core to 4d, which implies the explicit calculation of 14 additional electrons per platinum atom, has been shown to increase the adsorption energy by only about 5 kJ/mol for the adsorption of benzene.<sup>55</sup> The importance of relativistic effects has been shown for calculations involving platinum;<sup>56,57</sup> therefore, the core was modeled using a relativistically corrected core potential created with the DIRAC utility of the ADF program. The DIRAC calculations imply the local density functional in its simple X- $\alpha$  approximation without any gradient correction, but the fully relativistic Hamiltonian is used, including spin–orbit coupling. Furthermore, the relativistic scalar approximation (mass–velocity and Darwin corrections) was used for the Hamiltonian, with the zero-order regular approximation (ZORA) formalism,<sup>58–62</sup> where spin–orbit coupling is included already in zero order. The first-order Pauli formalism<sup>63</sup> was shown to have theoretical deficiencies due to the behavior of the Pauli Hamiltonian at the nucleus, which lead to variational collapse for increasing basis set size.<sup>64</sup> It was shown that the scalar relativistic correction could account for up to 70% of the total energy in the adsorption of carbon monoxide on platinum, and that also the calculated adsorption site was influenced by the use of relativistic corrections.<sup>56</sup> The ZORA formalism requires a special basis set, to include much steeper core-like functions, that are implemented in the code. Within this basis set, the double- $\zeta$  (DZ) basis functions were used for platinum, and double- $\zeta$  plus polarization (DZP) basis functions for the second row elements. The local part of the exchange and correlation functional was modeled using a Vosko, Wilk, Nusair parametrization of the electron gas.<sup>65</sup> The nonlocal part

**Scheme 2.** Reaction Scheme for the Hydrogenation of **1**



of the functional was modeled using the Becke correction for the exchange<sup>66</sup> and the Perdew correction for the correlation.<sup>67</sup> Energies were compared by setting as reference the most stable structure, because only relative energies were of interest for this work, and its values have been shown to be more reliable (less variation with the method used) than absolute ones.<sup>55</sup> All calculations were run unrestricted. To partially account for the surface reaction to the adsorbates, the central seven platinum atoms of the cluster were set free to optimize, while the other bond distances for platinum were fixed to the experimental value of 2.775 Å for bulk metal.<sup>68</sup> Molden<sup>69</sup> was used as graphical interface.

## Results

**Catalytic Experiments.** In the hydrogenation of **1**, the chemoselectivity to **1b** (Scheme 2) was only 25% in acetic acid and 79% in toluene. Addition of small amounts of achiral or chiral amines (modifiers) enhanced the chemoselectivity up to 100%; the results in the weakly polar solvent toluene are shown in Table 1. As compared to the unmodified hydrogenation, both chiral modifiers CD and (*R,R*)-PNEA (Scheme 1) enhanced the reaction rate even at low concentration (modifier/**1** = 0.0037 mol/mol). Interestingly, CD almost doubled the yield to **1b**, although quinuclidine (the function of CD that interacts with the substrate) barely affected the reaction and quinoline (the anchoring moiety of CD) diminished the yield remarkably when they were applied alone in the same concentration. The highest rate of the formation of **1b** was observed in the presence of MeOCD, the derivative of CD which is a more effective modifier of Pt in this reaction than the parent alkaloid (Figure 1).

Considering only the achiral amines, there is a positive correlation between the  $\text{pK}_a$  values of the amines and the rates of the target reaction. At 10-fold higher concentration, all amines enhanced the hydrogenation rate relative to the unmodified reaction. Note that tertiary amines can induce rate acceleration also in the Pt-catalyzed hydrogenation of ethyl pyruvate,<sup>70–72</sup> although the reliability of those observations has been questioned recently.<sup>73</sup>

A more detailed analysis revealed that the effect of amines was strongly concentration-dependent, as illustrated by some examples in Figures 1 and 2. In all cases, the reaction rate

(53) Frisch, M. J.; et al. *Gaussian 98*, A.7 ed.; Gaussian, Inc.: Pittsburgh, PA, 1998.

(54) Baerends, E. J.; et al. *ADF – Amsterdam Density Functional*, Release 2004-01 ed.; Scientific Computing and Modelling NV – Vrije Universiteit; Theoretical Chemistry: Amsterdam, 2004.

(55) Saeyns, M.; Reyniers, M.-F.; Marin, G. B.; Neurock, M. *J. Phys. Chem. B* **2002**, *106*, 7489.

(56) Philippen, P. H. T.; van Lenthe, E.; Snijders, J. G.; Baerends, E. J. *Phys. Rev. B* **1997**, *56*, 13556.

(57) Pacchioni, G.; Chung, S. C.; Kruger, S.; Rosch, N. *Surf. Sci.* **1997**, *392*, 173.

(58) van Lenthe, E.; Baerends, E. J.; Snijders, J. G. *J. Chem. Phys.* **1993**, *99*, 4597.

(59) van Lenthe, E.; Baerends, E. J.; Snijders, J. G. *J. Chem. Phys.* **1994**, *101*, 9783.

(60) van Lenthe, E.; Baerends, E. J.; Snijders, J. G. *J. Chem. Phys.* **1996**, *105*, 6505.

(61) van Lenthe, E.; van Leeuwen, R.; Baerends, E. J.; Snijders, J. G. *Int. J. Quantum Chem.* **1996**, *57*, 281.

(62) van Lenthe, E.; Baerends, E. J.; Snijders, J. G. *J. Chem. Phys.* **1999**, *110*, 8943.

(63) Snijders, J. G.; Baerends, E. J.; Ros, P. *Mol. Phys.* **1979**, *38*, 1909.

(64) te Velde, G.; Bickelhaupt, F. M.; Baerends, E. J.; Guerra, C. F.; van Gisbergen, S. J. A.; Snijders, J. G.; Ziegler, T. *J. Comput. Chem.* **2001**, *22*, 931.

(65) Vosko, S. H.; Wilk, L.; Nusair, M. *Can. J. Phys.* **1980**, *58*, 1200.

(66) Becke, A. D. *Phys. Rev. A* **1988**, *38*, 3098.

(67) Perdew, J. P. *Phys. Rev. B* **1986**, *33*, 8822.

(68) Somorjai, G. A. *Introduction to Surface Chemistry and Catalysis*; Wiley: New York, 1994.

(69) Schaftenaar, G.; Noordik, J. H. *J. Comput.-Aided Mol. Des.* **2000**, *14*, 123.

(70) Margittfalvi, J. L.; Hegedüs, M. *J. Catal.* **1995**, *156*, 175.

(71) Blaser, H. U.; Jalett, H. P.; Monti, D. M.; Reber, J. F.; Wehrli, J. T. *Stud. Surf. Sci. Catal.* **1988**, *41*, 153.

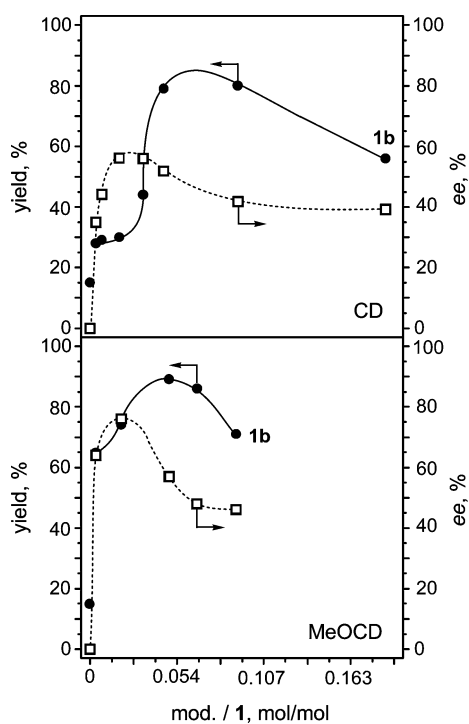
(72) Bond, G.; Meheux, P. A.; Ibbotson, A.; Wells, P. B. *Catal. Today* **1991**, *10*, 371.

(73) Toukoniitty, E.; Murzin, D. Y. *Catal. Lett.* **2004**, *93*, 171.

**Table 1.** Hydrogenation of **1** in the Presence of Achiral and Chiral Amines (Standard Conditions, Toluene)

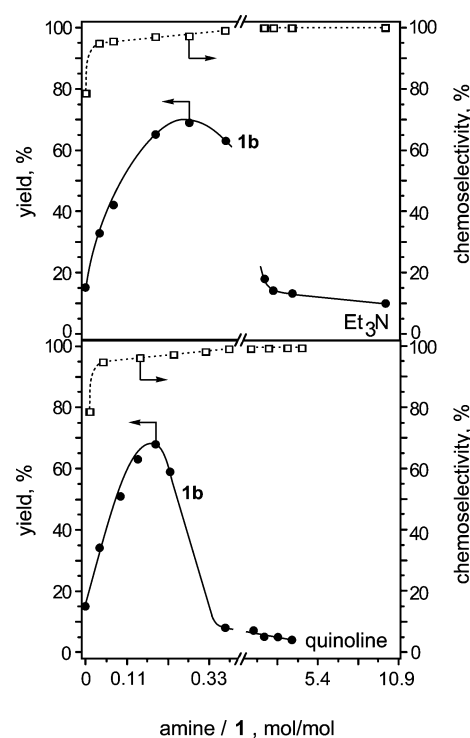
modifier	$pK_a$	mod/1 ratio [%]	conv. [%]	yields [%]		
				1a	1b	1c
			10	2	15	2
Me <sub>3</sub> N	9.80	0.37	11	n.d. <sup>a</sup>	11	n.d.
Et <sub>3</sub> N	10.72	0.37	13	n.d.	13	n.d.
quinuclidine	11.29	0.37	18	1	15	2
quinoline	4.94	0.37	4	n.d.	4	n.d.
( <i>R,R</i> )-PNEA		0.37	23	n.d.	23	n.d.
CD		0.37	28	n.d.	28	n.d.
MeOCD		0.37	66	n.d.	66	n.d.
Me <sub>3</sub> N	9.80	3.7	33	1	29	3
Et <sub>3</sub> N	10.72	3.7	38	1	33	4
quinuclidine	11.29	3.7	60	1	56	3
quinoline	4.94	3.7	37	1	34	2

<sup>a</sup> Not detectable (<0.2%).

**Figure 1.** The influence of the concentration of CD and MeOCD on the yield and enantioselectivity in the hydrogenation of **1** to **1b** on Pt/Al<sub>2</sub>O<sub>3</sub>; standard conditions, in toluene.

characterized by the yield to **1b** went through a maximum and at sufficiently high concentration the yield dropped below 15% achieved in the reference (unmodified) reaction. This apparent catalyst poisoning is attributed to a too high coverage of the active Pt sites by the amines, which leads to a reduced number of free sites available for the target reaction. As compared to CD and MeOCD, the rate acceleration was smaller with Et<sub>3</sub>N and quinoline and the maximum of the reaction rate was shifted to lower amine/substrate ratios. The chemoselectivity reached 100% at low chiral amine concentrations (CD, MeOCD, and (*R,R*)-PNEA, Table 1), while it increased monotonically in the presence of achiral amines up to relatively high amine/substrate ratios (Figure 2). The modifier concentration influenced also the enantioselectivity; the highest ee's in these series were 57% for CD and 76% for MeOCD.

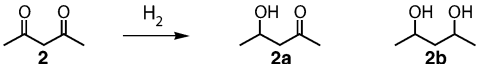
In summary, amines can accelerate the hydrogenation of the activated and suppress the transformation of the nonactivated keto group of **1** (Scheme 2). The achiral amines Me<sub>3</sub>N, Et<sub>3</sub>N,

**Figure 2.** The influence of the concentration of Et<sub>3</sub>N and quinoline on the yield and chemoselectivity to **1b** in the hydrogenation of **1** on Pt/Al<sub>2</sub>O<sub>3</sub>; standard conditions, in toluene.

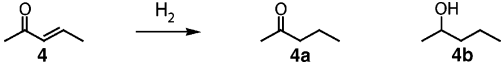
quinuclidine, and quinoline mimic the influence of CD, MeOCD, and (*R,R*)-PNEA, although they are less efficient than the chiral modifiers.

To clarify the role of the CF<sub>3</sub> group in the reactivity of **1**, acetylacetone (**2**) was also hydrogenated in the presence and absence of CD (Table 2). In contrast to the hydrogenation of **1**, the reaction rate decreased by the addition of CD irrespective of the solvent. The small but well reproducible ee reveals that the position of the quinuclidine N of CD relative to that of **2** adsorbed on the Pt surface is not symmetric. A possible explanation may be that not the keto but the enol form of **2** interacts with CD in the enantio-differentiating step.

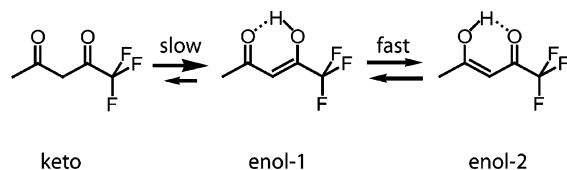
It was assumed earlier that in the enantioselective hydrogenation of the  $\beta$ -ketoester ethyl-4,4,4-trifluoroacetoacetate the keto carbonyl group rather than the C=C bond of the enol form was the reactive species on cinchona-modified Pt.<sup>22</sup> This assumption is in agreement with all mechanistic models developed for the enantioselective hydrogenation of activated ketones on Pt,

**Table 2.** Enantioselective Hydrogenation of Acetylacetone (**2**) on Unmodified and CD-Modified Pt/Al<sub>2</sub>O<sub>3</sub> (Standard Conditions)


modifier	solvent	conv %	2a		2b
			yield %	ee %	yield %
	toluene	29	17		12
CD	toluene	8	7	8 (R)	1
	dichloromethane	21	16		5
CD	dichloromethane	7	6	4(R)	1

**Table 3.** Hydrogenation of 3-Penten-2-one (**4**) on Unmodified and CD-Modified Pt/Al<sub>2</sub>O<sub>3</sub> (CH<sub>2</sub>Cl<sub>2</sub> Solvent and Standard Conditions)


modifier	conv %	yields %	
		4a	4b
	100	97	3
CD	100	99	1

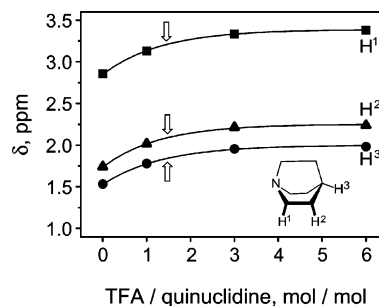
**Scheme 3.** Keto–Enol Equilibrium for **1**

although no experimental evidence could be found yet to support this hypothesis.<sup>6</sup> To estimate the reactivity of the C=C and C=O bonds in the enol forms of **2**, the hydrogenation of an analogous compound 3-penten-2-one (**4**) was investigated under standard conditions (Table 3). The C=C bond was completely saturated in 2 h, while the hydrogenation of the carbonyl group barely took place. Obviously, the reactivity of the C=C bond is much higher than that of the (deactivated) carbonyl group of **4**, and thus the reactivity of one of the enol forms of **1** (Scheme 3) on Pt cannot be excluded.

**NMR Study.** β-Diketones can be present in a keto- and two enol-forms (Scheme 3), and the keto–enol equilibrium depends on the solvent.<sup>74,75</sup> In weak to medium polar solvents, **1** exists mainly in its enol form (98% in toluene and 93% in dichloromethane).<sup>32</sup> The amount of enol-1 and enol-2 in solution can be quantified in CDCl<sub>3</sub> using the formula:

$$p_{\text{Me}} = (208 - \delta_{\text{Me}})/33 \quad (1)$$

where  $\delta_{\text{Me}}$  represents the chemical shift of the nonactivated carbonyl group in the <sup>13</sup>C NMR and  $p_{\text{Me}}$  indicates the amount of enol form on the side of the methyl group (enol-2).<sup>76</sup> Using this equation, we found that enol-1 was the dominant species (59%) in CDCl<sub>3</sub>. The slight shift of the equilibrium toward enol-1 is due to the presence of the electron-withdrawing CF<sub>3</sub> group.<sup>77</sup>

**Figure 3.** <sup>1</sup>H NMR investigation of the protonation of quinuclidine by **1** and TFA in CDCl<sub>3</sub>. The arrows mark the chemical shifts for a 1:1 mixture of **1** and quinuclidine. The concentration of **1** mimics the conditions in the general reaction procedure (0.37 mol/L).

Addition of an amine to **1** in solution leads to the formation of a protonated amine–enolate salt.<sup>78–80</sup> <sup>1</sup>H NMR investigation on the protonation of quinuclidine by **1** and trifluoroacetic acid (TFA) is shown in Figure 3. At least 4–6 mol equiv of TFA was necessary for complete protonation of quinuclidine in CDCl<sub>3</sub>. As compared to the shifts in the TFA/quinuclidine mixture, a strong acidity of the enolic proton of **1** can be estimated in this weakly polar medium.

Furthermore, the <sup>1</sup>H NMR spectrum of **1** in CDCl<sub>3</sub> shows a broad signal at  $\delta = 14.15$  ppm, which belongs to the enolic proton. After the addition of 1 mol equiv of quinuclidine, the signal of the enolic proton disappeared and a new signal appeared at 9.76 ppm (protonated nitrogen).

These NMR results confirm the strong acid–base interaction between **1** and quinuclidine. There was no signal in the NMR spectra giving evidence for a nucleophilic interaction between the quinuclidine N and the electrophilic carbonyl C atom and no zwitterion formation could be detected, in contrast to former reports on the interaction of  $\alpha,\alpha,\alpha$ -trifluoro-ketones and quinuclidine.<sup>23,37</sup>

The <sup>13</sup>C NMR signals of the two carbonyl carbons of **1** were found at 194.76 ppm (–COCH<sub>3</sub>) and at 176.05 ppm (–COCF<sub>3</sub>). After addition of 1 mol equiv of quinuclidine, the signal of the activated carbonyl group shifted upfield to 168.84 ppm, whereas the signal of the nonactivated carbonyl group remained constant at 194.82 ppm. Further increase of the amount of quinuclidine to 3 equiv had no influence on the chemical shifts, indicating a 1:1 interaction.

**FTIR Spectroscopy.** The infrared spectrum of **1** in CH<sub>2</sub>Cl<sub>2</sub> (Figure 4) displays bands at ca. 1645, 1601, 1206, 1157, and 1109 cm<sup>–1</sup>, together with a weak envelope at around 1790 cm<sup>–1</sup>. This last feature is given by the  $\nu(\text{C}=\text{O})$  mode of the free diketone species, which however account only for about 7% of the species in solution.<sup>32</sup> The spectrum of compound **1** is predominantly a combination of the spectra of the two enol forms, whose calculated vibrational spectra are reported in Figure 4c and d scaled by 0.967. The spectra agree well with those already available in the literature.<sup>81</sup> The linear combination of the calculated vibrational spectra of the two enol forms in the ratio 41:59 in favor of enol-1, as suggested by the <sup>1</sup>H NMR data, matches the experimental spectrum of **1**. According to the

(74) Emsley, J. *Structure and Bonding, Complex Chemistry: The Composition, Structure and Hydrogen Bonding of the β-Diketones*; Springer-Verlag: Berlin, 1984.

(75) Rogers, M. T.; Burdett, J. L. *Can. J. Chem.* **1965**, *43*, 1516.

(76) Koltsov, A. I. *J. Mol. Struct.* **1998**, *444*, 1.

(77) Niwa, J.; Yamazaki, M.; Takeuchi, T. *Chem. Lett.* **1975**, *4*, 707.

(78) Koltsov, A. I.; Golubev, N. S.; Milevskaya, I. S. *Zh. Obshch. Khim.* **1980**, *50*, 2504.

(79) Pashkevich, K. I.; Filyakova, V. I. *Bull. Acad. Sci. USSR* **1984**, *33*, 575.

(80) Filyakova, V. I.; Ratner, V. G.; Karpenko, N. S.; Pashkevich, K. I. *Russ. Chem. Bull.* **1996**, *45*, 2163.

(81) Minoura, Y.; Nagashima, N.; Kudoh, S.; Nakata, M. *J. Phys. Chem. A* **2004**, *108*, 2353.

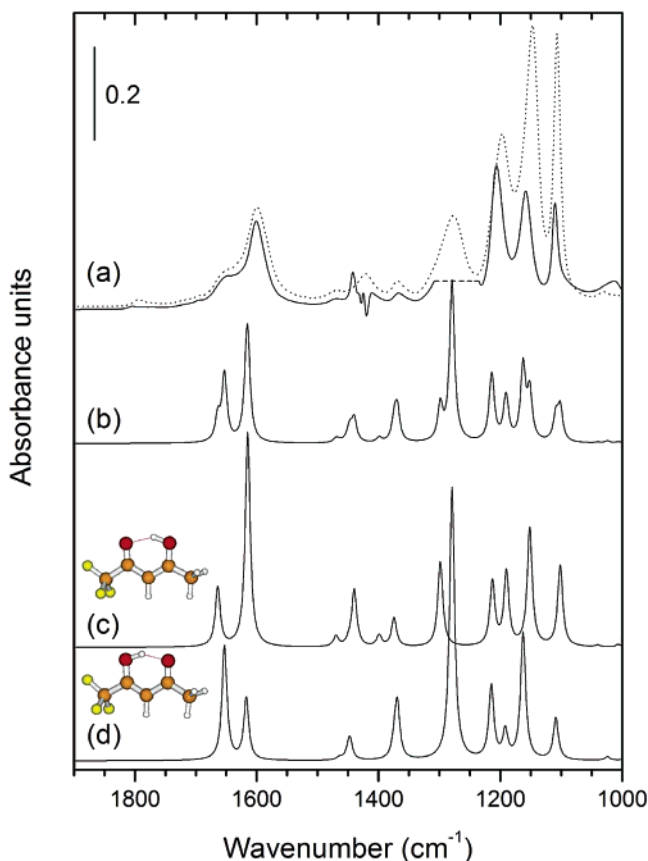


**Figure 4.** Experimental and calculated vibrational spectra of **1**. (a) Transmission IR spectrum of a solution of **1** in  $\text{CH}_2\text{Cl}_2$  (5 mM). Calculated vibrational spectra (scaled by 0.967) of (b) a mixture of the enol forms 59:41, (c) enol-2, and (d) enol-1 forms. (b) Vibrational spectrum obtained by combining the calculated vibrational spectra of the two enol forms in the ratio 59:41. The dotted spectrum in (a) corresponds to neat **1**.

calculated vibrational spectra, the signals at 1645 and 1601  $\text{cm}^{-1}$  correspond to the asymmetric and symmetric stretching motions of the C=O and C=C groups, whereas the set of signals between 1250 and 1100  $\text{cm}^{-1}$  is assigned to the vibrational modes associated with the  $\text{CF}_3$  and CH groups.

The infrared spectrum of **1** exhibited striking changes upon titration of a solution of **1** with a solution of quinuclidine (Figure 5a). In the high-frequency region (left panel), a broad band centered at 2640  $\text{cm}^{-1}$  increased with increasing quinuclidine concentration. The changes observed in the middle panel of Figure 5a suggest the immediate disappearance of the free diketone species (1790  $\text{cm}^{-1}$ ) and the replacement of the bands at 1645 and 1601  $\text{cm}^{-1}$  by signals at 1640 and 1530  $\text{cm}^{-1}$ , respectively, at 1 mol equiv of base. In the right panel of Figure 5a, the signals at 1157 and 1109  $\text{cm}^{-1}$  disappeared almost completely upon addition of quinuclidine, whereas new signals were found at 1175 and 1128  $\text{cm}^{-1}$ . The signal at 1206  $\text{cm}^{-1}$  is strongly attenuated. Two isosbestic points can be clearly observed at 1167 and 1113  $\text{cm}^{-1}$  that indicate the transition from the species related to the spectrum before addition of quinuclidine (dotted) to new species formed after addition of the base (bold spectrum).

Figure 5b shows that the interaction between CD and **1** is identical to that between quinuclidine and **1**, with only minor differences in the position of the new signals. The additional signals at 1593, 1572, and 1510  $\text{cm}^{-1}$  (quinoline ring modes)

and at 3594  $\text{cm}^{-1}$  ( $\nu(\text{O}-\text{H})$ ) are characteristic of the alkaloid.<sup>82</sup> The presence of the mode of the free OH group of CD indicates that this function is not involved in the interaction with **1**.

The spectral changes observed upon titration of **1** by quinuclidine (and CD) are associated with the formation of the ion pair composed of the quaternary ammonium ion of quinuclidine (2600  $\text{cm}^{-1}$ ) and the enolate anion of **1** (1640, 1530, 1204, 1175, and 1128  $\text{cm}^{-1}$ ).<sup>79,82,83</sup> The two major bands at 1640 and 1530  $\text{cm}^{-1}$  belong to groups displaying C=O<sup>79</sup> and C=C character. Although deprotonation of **1** does not allow the localization of the two bonds (formation of the enolate ion), the presence of molecular asymmetry in **1** induced by the  $\text{CF}_3$  group suggests that the charge distribution between the O-atoms is also asymmetric.

This last observation becomes particularly important for the discussion on how the chemoselectivity is controlled upon addition of the chiral amine during the enantioselective hydrogenation of **1**. Therefore, interpretation of the changes observed in Figure 5a (and Figure 8b, see later) required the aid of vibrational analysis to resolve the structure of the enolate ion and clarify which C–O bond has a partial C=O character in the ion pair, the information of which is missing from the available literature. Theoretical calculations were carried out enabling the relaxation of the proton located on the amine toward one of the two O-atoms of the enolate. The structure is shown in the inset of Figure 5 together with the calculated spectrum of the acid–base pair **1**: $\text{Me}_3\text{N}$ , which matches well the experimental spectrum in Figure 5a. The frequency of the sharp signal at 1951  $\text{cm}^{-1}$  (calcd 2018  $\text{cm}^{-1}$ ) for the  $\nu(\text{N}-\text{H}^+)$  mode is underestimated as compared to the other vibrations probably due to the fact that the calculations localize the proton on the N-atom. Interestingly, the vibrational analysis suggests that the C–O on the side of  $\text{CF}_3$  rather than that on the side of  $\text{CH}_3$  has a partial C=O character. The signals at 1640 and 1530  $\text{cm}^{-1}$  are then assigned to  $\nu(\text{C}_{\text{CF}_3}-\text{CO})+\nu(\text{C}-\text{C}_{\text{CH}_3})$  and  $\nu(\text{C}-\text{C}_{\text{CH}_3})+\nu(\text{C}_{\text{CF}_3}-\text{CO})$  modes of the enolate of **1**, respectively.

Figure 6 shows the FTIR spectra of solutions of the diketones **1**, **2**, and **3** before and after addition of 1 mol equiv of amine. The least reactive substrate toward deprotonation, that is, the least acidic, is **2**, in agreement with the effect induced by substitution of a  $\text{CH}_3$  group by a  $\text{CF}_3$  group. In the FTIR spectra of the neat substrates, this substitution results in the splitting of the signals assigned to the asymmetric and symmetric stretching of the  $\text{O}=\text{C}-\text{C}=\text{C}-\text{O}$  group<sup>84</sup> and in the complete disappearance of the free diketone species in the case of **3**.<sup>85</sup>

Addition of quinuclidine does not affect the spectrum of **2** but substantially alters the spectra of **1** and **3**. As in the case of the ion pair **1**:quinuclidine, the signals at 1666 and 1549  $\text{cm}^{-1}$  in Figure 6f are attributed to the formation of the enolate of **3**. Additional signals are also found between 3000 and 2000  $\text{cm}^{-1}$  (broad,  $\nu(\text{N}-\text{H}^+)$ ) and at 1192, 1144, and 1136  $\text{cm}^{-1}$ . The enolate ions of **2** and **3** exist only in a single form due to molecular symmetry. The enolate of **2** in aqueous solution absorbs at frequencies below 1600  $\text{cm}^{-1}$ ,<sup>86,87</sup> that is, more than

(82) Ferri, D.; Bürgi, T.; Baiker, A. *J. Chem. Soc., Perkin Trans. 2* **1999**, 1305.

(83) Bellamy, L. J. *The Infrared Spectra of Complex Molecules. Advances in Infrared Group Frequencies*; Chapman and Hall: London, 1980; Vol. 2.

(84) Ogoshi, H.; Nakamoto, K. *J. Chem. Phys.* **1966**, *45*, 3113.

(85) Wallen, S. L.; Yonker, C. R.; Phelps, C. L.; Wai, C. M. *J. Chem. Soc., Faraday Trans.* **1997**, *93*, 2391.

(86) Ernstrunner, E. E. *J. Chem. Soc. A* **1970**, 1558.

(87) Dickie, S. A.; McQuillan, A. *J. Langmuir* **2004**, *20*, 11630.

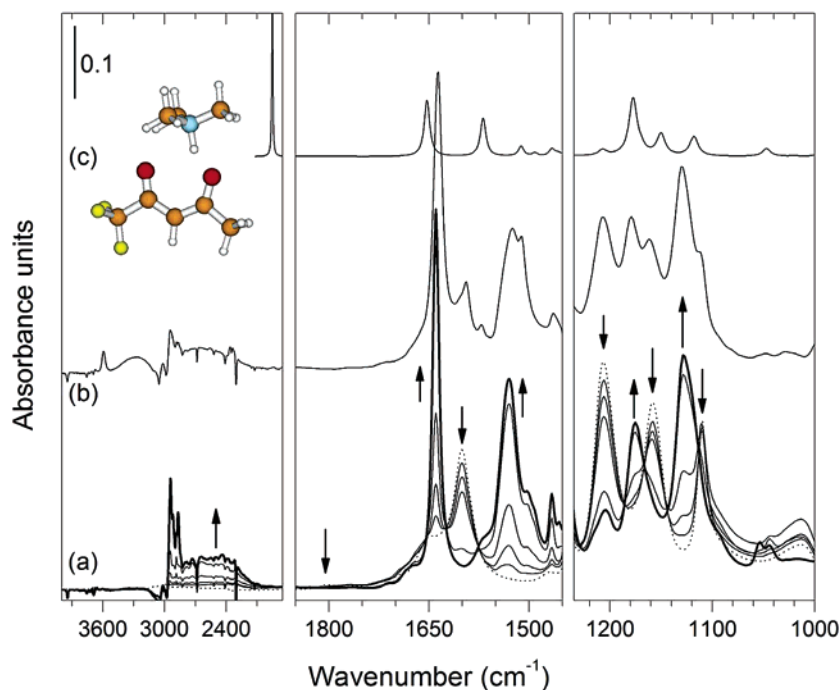


**Figure 5.** Transmission infrared spectra of a solution of (a) **1** with 0 (dotted), 0.1, 0.2, 0.4, 1, and 2 (bold) equiv of quinuclidine and (b) **1** with 1 equiv of CD. Arrows indicate the direction of the changes upon base addition. The calculated vibrational spectrum of the complex **1**:Me<sub>3</sub>N is shown in (c) (scaling factor 0.967). Spectra b and c are offset.  $C_1 = C_{CD} = 5$  mM,  $C_{amine} = 0.5, 1, 2, 5,$  and 10 mM, ambient temperature, in CH<sub>2</sub>Cl<sub>2</sub>.

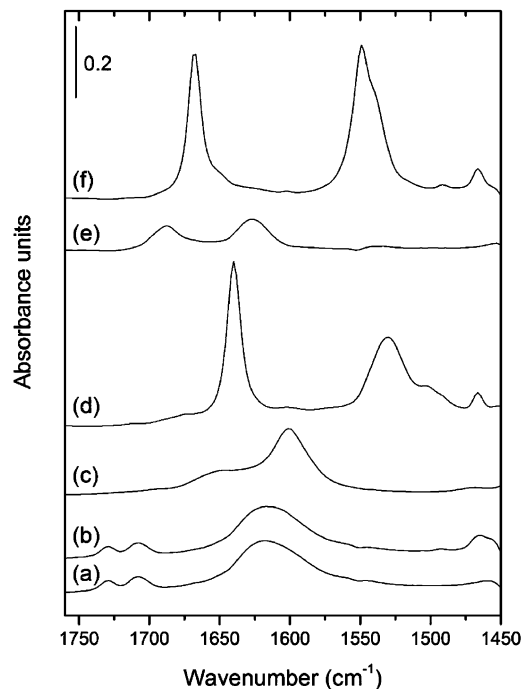


**Figure 6.** FTIR spectra of solutions of (a) **2**, (c) **1**, and (e) **3**. Addition of 1 equiv of quinuclidine afforded spectra b, d, and f, respectively.  $C = 5$  mM, ambient temperature, in CH<sub>2</sub>Cl<sub>2</sub>.

$40\text{ cm}^{-1}$  below the frequency observed for the enolate of **1**. The enolate of **3** exhibits the  $\nu(\text{C}=\text{O})$  at  $1666\text{ cm}^{-1}$  and shows a  $\Delta\nu$  with respect to the enolate of **1** of only  $26\text{ cm}^{-1}$ . The difference in shift suggests that the enolate of **1** resembles more the enolate of **3** and displays some carbonyl character on the C–O bond near the CF<sub>3</sub> group, in agreement with the usually observed blue-shift of the  $\nu(\text{C}=\text{O})$  band of ketones upon

introduction of the electron-withdrawing CF<sub>3</sub> group, thus further supporting the validity of the vibrational analysis of the ion pair.

**Adsorption of 1 on Pt.** Adsorption of **1** was studied using a Pt 31 cluster to model the surface to better understand the catalytic behavior. Figure 7a shows the adsorption mode of **1** in the diketo-form, chemisorbed  $\eta^2$  via the activated keto-carbonyl group (i.e., the keto-carbonyl in  $\alpha$ -position to the CF<sub>3</sub> group). The other possibility, the adsorption of the diketo-form chemisorbed  $\eta^2$  via the nonactivated keto-carbonyl group, is presented in Figure 7b. Consistently with previous results,<sup>88</sup> the former was more strongly adsorbed by ca. 3 kcal/mol than the latter. This result was rationalized by the energy lowering of the frontier orbitals of the activated keto-carbonyl, which can better interact with the filled states of the metal in back-bonding interactions.<sup>88,89</sup> This chemisorption mode of C=O double bonds is also called di- $\sigma$  to evidence the double  $\sigma$  binding of the keto carbonyl moiety to the metal atoms. Also,  $\eta^1$  adsorption modes are theoretically possible, but it has been shown that their adsorption energy is much smaller than the  $\eta^2$  modes, and, in particular, in such adsorption modes the keto-carbonyl moiety is distant from the surface and cannot reach surface hydrogen; therefore, they are less interesting in our discussion.<sup>88</sup> On the other hand, the  $\eta^2$  modes show rehybridization of the keto-carbonyl group and have the right geometry for hydrogen uptake. Another adsorption mode of the diketo-form is shown in Figure 7c, where the diketone is adsorbed with both carbonyl groups close to the surface. Because both carbonyls cannot simultaneously find an optimal interaction with the surface Pt atoms, the most strongly interacting moiety dominates the adsorption. This mode is energetically disfavored as compared to the two previous structures; nevertheless, we observe that the result of this interaction is the rehybridization of the activated

(88) Vargas, A.; Bürgi, T.; Baiker, A. *J. Catal.* **2004**, *222*, 439.

(89) Hammer, B.; Nørskov, J. K. *Adv. Catal.* **2000**, *45*, 71.

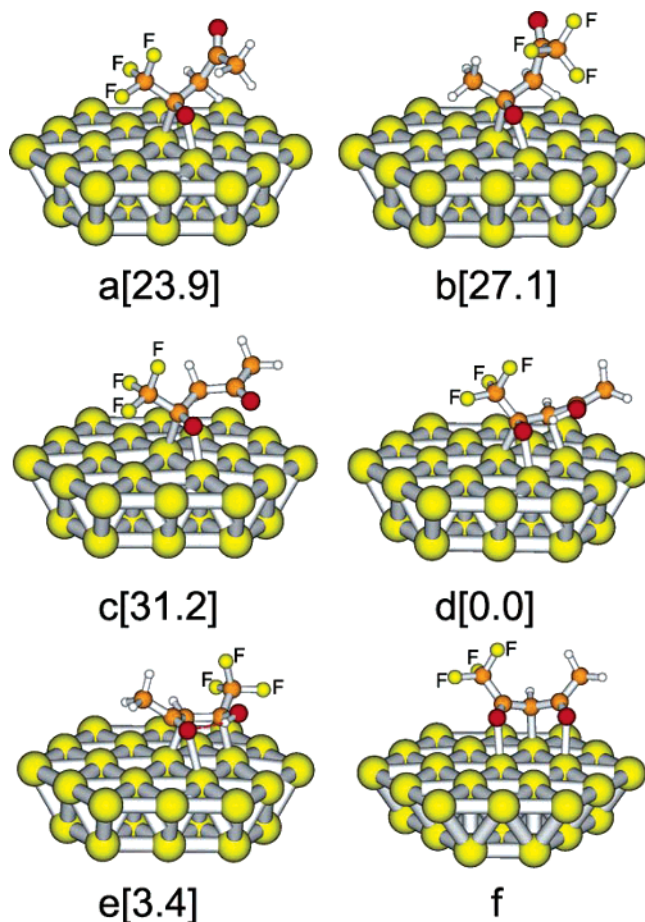


**Figure 7.** Calculated adsorption modes of **1** on a Pt cluster. Structures (a), (b), and (c) show the adsorption of the diketo-form, (d) and (e) the adsorption of the enol forms, and (f) the adsorption of the enolate. The energy of the most stable structure (d) has been set to zero and taken as a reference for the others. The numbers in brackets are the energy differences (kcal/mol) between (d) and the other (less stable) structures.

keto-carbonyl only, although also the nonactivated carbonyl is close to the metal.

The adsorption of the enol forms of **1** (Figure 7d and e) was the most energetically favored, with a preference for the adsorption of enol-2 (Figure 7d), where the optimal chemisorption of the activated carbonyl is possible. It should be noted that the adsorption of enol-1 (Figure 7e) does not lead to the expected  $\eta^2$  interaction of the nonactivated carbonyl with the metal, but rather with the formation of a  $\sigma$ -bond between the carbon neighboring the  $\text{CF}_3$  group and a Pt atom. Also, in this case, the competition for surface sites is in favor of the activated carbonyl group, and the result is that the nonactivated carbonyl undergoes no evident structural alteration induced by the metal. Also, to be noted is that both adsorbed enol forms are stabilized by internal hydrogen bonds. However, while in enol-2 the H-bond length is 1.35 Å, it elongates to 1.71 Å in enol-1, showing the stronger hydrogen-acceptor character of the adsorbed activated carbonyl group.

The structures of the diketo and enol forms without surface interaction were also calculated using the same level of theory. The two conformations of the diketo-form (not shown) are about 10 and 15 kcal/mol, respectively, less stable than the lowest energy enol-2 at this level of theory. For our purposes, it is important to note that after chemisorption the difference in energy between the enol and keto forms of **1** is greatly enhanced

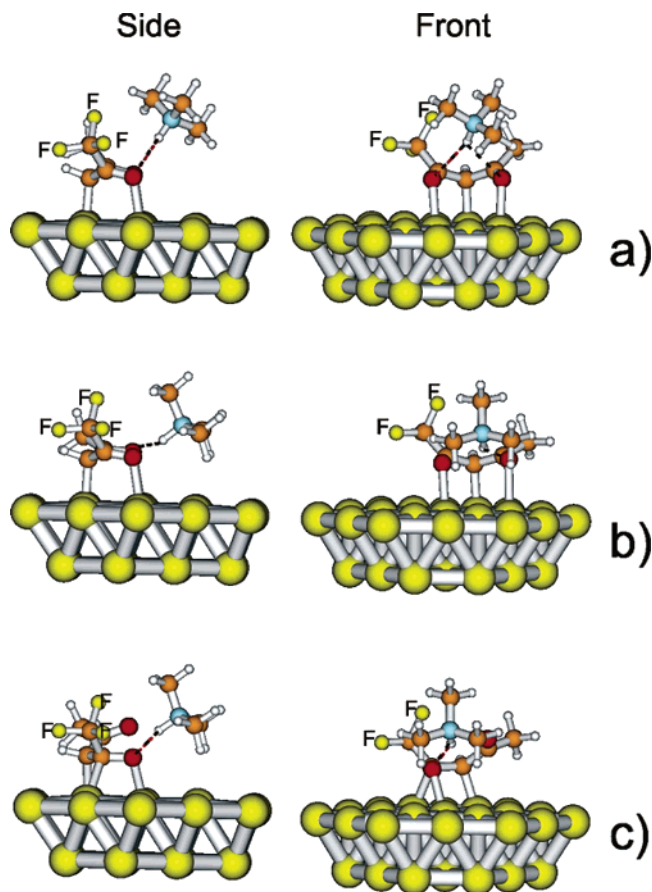


**Figure 8.** Simulation of the interaction between  $\text{Me}_3\text{NH}^+$  and adsorbed enolate. Structure (a) is the starting geometry, in which the acidic proton is equidistant from the two oxygen atoms. Structure (b) is an intermediate point of the optimization, where the  $\text{Me}_3\text{NH}^+$  is closer to the nonactivated moiety and removes it from the surface. Structure (c) is the converged geometry, where the  $\text{Me}_3\text{NH}^+$  is coordinated to the di- $\sigma$  adsorbed CO.

with respect to the molecules that are not interacting with the metal. Binding to the metal increases the difference of stability by a factor of 2, raising it to 20 and 30 kcal/mol in favor of the enol forms.

Figure 7f shows the adsorption mode of the enolate, the deprotonated form of the enol, thus a charged species. Unlike the enols, the enolate has a more symmetric adsorption mode where both oxygen atoms are bound to a metal atom, and with a third  $\sigma$  binding site due to C(3) that is also bound to a metal atom and rehybridized. Note that the relative energy is not given, because this structure contains one hydrogen less than the others and its energy cannot be simply compared. The negative charge of the enolate is delocalized on the metal upon adsorption.

It has been discussed previously that introducing an amine in the reaction system leads to an almost complete chemoselectivity in the saturation of the activated keto-carbonyl group of **1**. It has also been shown that in solution the amine deprotonates the enol and generates an ammonium ion and the enolate. Therefore, the interaction between the trimethylammonium ion and the enolate was modeled in the presence of the Pt surface. Figure 8 shows three steps of this simulation: Figure 8a shows the starting geometry whereby the (trimethyl)-ammonium ion is positioned close to the adsorbed enolate ion, such that the distance between its acid hydrogen and the oxygen atoms of the enolate is equal (2.5 Å). During minimization, the ammonium ion moves toward the surface and comes closer to



the nonactivated CO, as shown in Figure 8b. In this intermediate position, the hydrogen bond formed with the nonactivated moiety is 1.8 Å, while that formed with the activated moiety is 2.3 Å. As the optimization continues, this preferential coordination leads to a displacement of the nonactivated keto-carbonyl from the surface, and when convergence is reached the ammonium ion coordinates the activated CO bond that changes its adsorption mode to  $\eta^2$  (Figure 8c).

## Discussion

A big effort has been made in past years to understand the functioning of chirally modified Pt in the enantioselective hydrogenation of ketones. As discussed in the Introduction, several mechanistic models have been proposed, but only one of these models is supported by in situ experimental observations.<sup>45</sup> A major difficulty is the high reactivity of activated ketones in the presence of amine-type modifiers that complicates or even hinders the study of substrate–modifier interactions in solution.<sup>90</sup> The present study is the first example where the nature of the amine–ketone interaction in solution could be refined by spectroscopic methods, and further modeled by state-of-the-art calculations.

The hydrogenation experiments have shown that both carbonyl groups are reactive on Pt that may lead to poor chemoselectivity, but only the activated carbonyl group is reduced to an alcoholic OH function in the presence of the chiral amine and amino alcohol-type modifiers CD, MeOCD, and (*R,R*)-PNEA (Table 1, Figure 1). The remarkable enhancement in chemoselectivity is due to acceleration of the hydrogenation of the activated and deceleration of the hydrogenation of the nonactivated carbonyl functions by the basic amine. It has also been proved by catalytic and spectroscopic methods that simple achiral amines (e.g., Me<sub>3</sub>N, Et<sub>3</sub>N, quinuclidine) could improve the chemoselectivity, although to a smaller extent (Figure 2), and the OH function of CD was not involved in the substrate–modifier interaction (Figures 4 and 5). The better efficiency of the chiral modifiers as compared to simple amines at identical (low) solution concentrations is attributed to the stronger adsorption of the modifiers on the Pt surface. Note that strong adsorption leading to high surface concentration is one of the key characteristics of effective chiral modifiers.

NMR and FTIR spectroscopy has revealed that, in contrast to former reports,<sup>91,92</sup> **1** is about as strong of a proton donor as TFA (Figure 3) and formation of the enolate-ammonium ion pair, where the quaternary ammonium ion coordinates to the enolate, is responsible for enantioselection. The structure assigned to this ion pair partially localized the proton between the N-atom of the amine and the O-atom of the nonactivated keto-carbonyl of **1**. For comparison, the small but significant ee observed in the hydrogenation of **2** (Table 2) indicated that the position of the N atom relative to the O atoms in the modifier–substrate complex is nonsymmetric even in the absence of the electronic effect of fluorine atoms.

A striking result of this study is that the substrate–modifier interaction identified in solution by spectroscopic methods cannot interpret the chemoselectivity observed in the hydroge-

nation of **1**. The real origin of enhanced chemoselectivity induced by addition of amines could be clarified only by considering the adsorption on the metal surface.

The theoretical study of the adsorption of the different (equilibrated) species of **1** on a model Pt cluster has shown that the enol forms are more stable also on the surface with respect to the diketo-form and adsorption even increased the difference in their stability (Figure 7). More interestingly, the simulation of the formation of the ion pair on the metal surface has revealed that coordination of the ammonium ion to the adsorbed enolate results in the displacement of the nonactivated CO from the metal surface and at the same time the promotion of an  $\eta^2$  adsorption mode of the activated CO. In the equilibrium geometry shown in Figure 8c, the ammonium ion coordinates to the activated CO moiety adsorbed  $\eta^2$ . It has already been proposed that  $\eta^2$  adsorption modes of ketones are more activated toward hydrogenation, and the results shown in Figure 8 seem to be in good agreement with this proposal.<sup>88</sup>

The apparent mismatch between the spectroscopic results obtained in solution and the adsorption study correctly interpreting the observed changes in chemoselectivity may be explained as follows. As mentioned, the ion pair formed with the ammonium ion and the enolate in solution is characterized by a closer interaction between the acidic proton and the nonactivated CO. This interaction is also present when the ion pair is interacting on the metal surface, but only in the first phase of the interaction (Figure 8b). In contrast, the activated CO, which is di- $\sigma$  adsorbed, dominates the interaction with the acidic proton at equilibrium, consistent with the electron transfer to the metal, making this group a better hydrogen-bond acceptor. Comparison of these results to the catalytic experiments strongly suggests that the ammonium ion promotes the hydrogenation of the activated keto-carbonyl by selective coordination, with a fundamental contribution from the metal surface enhancing its proton affinity that cannot be neglected. On the other hand, the calculated geometry of the enolate explains why hydrogenation of the nonactivated carbonyl lying well above the metal surface is hindered in the presence of an amine. This observation highlights the influence of the metal surface on the substrate–modifier interaction.

The unambiguous relation between chemoselectivity and metal–substrate–modifier interaction is valuable to assess the debated model of the interaction between cinchona alkaloids and activated ketones during enantioselective hydrogenation on cinchona-modified platinum. In fact, a similar N–H–O-type interaction is expected between the protonated quinuclidine moiety of the alkaloid and an adsorbed activated ketone substrate. This can occur also in a nonacidic medium (such as toluene). It has been shown recently that the alkaloid can be protonated by uptake of activated hydrogen from the Pt surface.<sup>44,45</sup>

The hydrogen-bonding interaction has already been interpreted as the trigger for rate acceleration,<sup>93,94</sup> which is observed also in the experiments discussed here. The enantioselectivity in the presence of the adsorbed modifier is to be interpreted as the result of different interaction energies that the prochiral faces of the ketone substrate show within a chiral environment

(90) Ferri, D.; Bürgi, T.; Borszky, K.; Mallat, T.; Baiker, A. *J. Catal.* **2000**, *193*, 139.

(91) Pashkevich, K. I.; Saloutin, V. I.; Postovskii, T. Y. *Russ. Chem. Rev.* **1981**, *50*, 180.

(92) Shukla, J. P.; Sharma, R. S. *Electrochim. Acta* **1986**, *31*, 1449.

(93) Vargas, A.; Bürgi, T.; Baiker, A. *New J. Chem.* **2002**, *26*, 807.

(94) Vargas, A.; Bürgi, T.; von Arx, M.; Hess, R.; Baiker, A. *J. Catal.* **2002**, *209*, 489.

generated by the alkaloid on the surface. As already proposed,<sup>93,94</sup> enantiodiscrimination should arise from two combined effects, both related to the strength of the hydrogen-bond interaction: on one hand, the best fitting prochiral face has the lowest energy and therefore a higher fractional coverage; on the other hand, the stronger hydrogen-bond interaction should show the largest rate enhancement, generating kinetic resolution. A quantification of the two effects is only possible via modeling of the interaction between the alkaloid and the substrate both adsorbed on the metal, which is the subject of ongoing investigation in our laboratory. The better performances obtained using cinchona alkaloids as carriers for the amino-group show the unique feature of these molecules that provide the reactive site (basic nitrogen) in proximity of the metal, still allowing the presence of free metal sites. The structural features of the cinchona alkaloids allow reshaping of the surface upon adsorption and generation of new surface sites without annihilation of the availability of the metal for the contact with the substrate, unlike quinoline (the “anchoring group” of the alkaloid), which is a catalyst poison when used alone (Table 1, Figure 2). Therefore, the cinchona alkaloids are properly called surface chiral modifiers, whereas a simple alkylamine is a reaction additive.

### Conclusions

Catalytic experiments combined with spectroscopic and computational structural analysis have been applied to understand the coupled phenomena: the enantioselection and the enhancement of chemoselectivity in the hydrogenation of the activated keto-carbonyl group of **1**. The study revealed that the structures of ammonium ion–enolate-type ion pairs formed

between the modifier and **1** are different in solution and on the Pt surface. The outstanding chemoselectivity is attributed to the selective coordination of the protonated amine (modifier) to the adsorbed activated keto-carbonyl group and prevention of the interaction of the nonactivated carbonyl group in this position with the metal surface. The fundamental differences in the structures of the substrate–modifier ion pair in solution and on the Pt surface underline that the reaction mechanism cannot be understood without considering the adsorption on the metal surface.

The presented model shows important similarities to those suggested for the enantioselective hydrogenation of other activated ketones on Pt modified by chiral amines.<sup>14,49,95</sup> In all cases, an N–H–O-type hydrogen bond between the amine modifier and the keto-carbonyl group of the adsorbed substrate is critical for rationalizing the outcome of the reaction, concerning both the rate enhancement and the enantioselectivity.

**Acknowledgment.** We kindly acknowledge the Swiss National Science Foundation for financial support and the Swiss Center for Scientific Computing (SCSC) in Manno and ETHZ for computing time.

**Supporting Information Available:** Detailed assignment of the vibrational modes of the two enol forms of **1** and of the **1**:Me<sub>3</sub>N, Cartesian coordinates of the structures shown in Figures 7 and 8, and full refs 53 and 54. This material is available free of charge via the Internet at <http://pubs.acs.org>.

JA057586F

(95) Bodmer, M.; Mallat, T.; Baiker, A. In *Catalysis of Organic Reactions*; Herkes, F. E., Ed.; M. Dekker: New York, 1998; p 75.